ARTICLE

Toward Understanding Amino Acid Adsorption at Metallic Interfaces: A Density Functional Theory Study

Gongyi Hong,[†,‡] Hendrik Heinz,[§] Rajesh R. Naik,[†] Barry L. Farmer,[†] and Ruth Pachter*[,†]

Air Force Research Laboratory, Materials & Manufacturing Directorate, Wright-Patterson Air Force Base, Ohio 45433-7702, General Dynamics Information Technology, Dayton, Ohio 45431, and Department of Polymer Engineering, The University of Akron, Akron, Ohio 44325-0301

ABSTRACT In examining adsorption of a few selected single amino acids on Au and Pd cluster models by density functional theory calculations, we have shown that specific side-chain binding affinity to the surface may occur because of a combination of effects, including charge transfer. Larger binding was calculated at the Pd interface. In addition, the interplay between amino acid solvation and adsorption at the interface was considered from first principles. This analysis serves as the first step toward gaining a more accurate understanding of specific interactions at the interface of biological–metal nanostructures than has been attempted in the past.

KEYWORDS: amino acid surface binding affinity • biological–metal interface • density functional theory

INTRODUCTION

A growing number of research efforts in which biomolecules are used to synthesize and assemble nanomaterials have been emerging recently (1–3). For example, nanoparticle synthesis using binding peptides, identified by phage display and showing compositional specificity (4), enabled a broad range of biosensing and bioelectronics applications (5), including protein-based components for nanodevices (6). It is therefore of increasing interest to gain a fundamental understanding of the interaction of peptides with inorganic surfaces. However, such insight has not been extensively gained as yet, particularly in systematic examination of the intrinsic affinity to metal surfaces.

Although Peelle et al. (7) studied design criteria for peptides binding Au by investigating homogeneous hexamers of the 20 naturally occurring amino acids in film substrates, the compositional specificity is not consistent, for example, with the binding of A3 (-Ala-Tyr-Ser-Ser-Gly-Ala-Pro-Pro-Met-Pro-Pro-Phe-), and Asp-rich Flg (-Asp-Tyr-Lys-Asp-Asp-Asp-Asp-Lys-) in solution, as recently observed experimentally (8). On the other hand, the data of Willett et al. (9), where adhesion of 8–10 mers of single amino acid types was examined for a broad range of surfaces in aqueous solution, including gold surfaces, indicates that both for A3 and Flg, the amino acids that compose the sequences are, in part, consistent with Au binding, specifically for Pro and Ser in A3, and Asp in Flg. Interestingly, peptide sequences that exhibit Pd binding, namely, (-Asn-Phe-Met-Ser-Leu-Pro-Arg-Leu-Gly-His-Met-His-), (-Thr-Ser-Asn-Ala-Val-His-Pro-Thr-Leu-Arg-His-Leu-), and (-Thr-Thr-Thr-Lys-Ser-Ile-Thr-Leu-Thr-Leu-Ser-Val-) (10), are also mostly consistent with the single amino acid-type data of Willett et al. (9), such as for hydrophilic Thr, basic Lys, His, and Arg amino acids' binding, and for nonpolar Met, Gly, and Val. However, some inconsistencies remain, and the difference between binding of A3 and Flg on Au and Pd (11) is still not well understood.

At the same time, theoretical examination of peptide–metal surface interactions is also rather limited. In previous molecular dynamics (MD) simulations using the CHARMM empirical potential, interactions of (-Met-His-Gly-Lys-Thr-Gln-Ala-Thr-Ser-Gly-Thr-Ile-Gln-Ser-) on Au were investigated (12). Although visual examination of the results has shown cases of close contact at the interface, such observations are not sufficient for understanding specific binding characteristics. Indeed, the need for applying first principles calculations to explain adsorption at inorganic surfaces has been recognized (13) and noted for metal surfaces (14).

On metal surfaces, adsorbate–metal binding leads to induced surface dipoles, causing a change in the work function of the metal, in turn related to the binding, which can be explained, in part, by exchangelike effects. The importance of exchange interactions upon physisorption on metals, for example, as shown for olefins on Ag(111) (15), or for C_6H_{12} on Cu(111), as based on MP2 calculations to better include also dispersion, was demonstrated (16). Depending on the adsorbed moiety, binding can also originate from charge transfer, as shown for instance for self-assembled monolayers of organothiolates on Ag(111) (17). In general, interface interactions originate from electrostatics, including charge transfer and induction, as well as exchange and dispersion. Empirically available parametriza-

* Corresponding author. E-mail: Ruth.Pachter@wpafb.af.mil.
Received for review October 6, 2008 and accepted November 30, 2008
[†] Wright-Patterson Air Force Base.
[‡] General Dynamics Information Technology.
[§] The University of Akron.
DOI: 10.1021/am800099z

Published on Web 01/06/2009

tion in atomistic classical simulations does not fully account for all contributions to the affinity for adsorption. Therefore, to discern effects of peptide adsorption on a metal surface, density functional theory (DFT) calculations were carried out, where contributions from charge transfer and exchange interactions upon adsorption were included. Note that our emphasis was on the effects of adsorption for a charged amino acid, and therefore no systematic examination of the relative electrostatic, exchange, and dispersion contributions to the total energy for periodic metal slabs upon side-chain adsorption was attempted. In future work, improvements in the functional that includes empirical dispersion (18) will be used, in order to explain interactions of all amino acids at a metal interface. Of course, empirical MD simulations are useful when examining structural aspects of a peptide without taking into account its binding to the surface, as shown when studying adsorption to a cuprous oxide surface, in an effort to investigate the role of the peptide's conformational context in binding (19), as has also been reviewed (20). Note that electronic properties of DNA base molecules on a metallic Cu(111) surface were also recently investigated (21), as well as on single-wall carbon nanotubes (22), assessing carefully the orientation of nucleotides on C(10,0).

In addition, interaction with the solvent has to be examined, for example, for analyzing the interplay between the water−amino acid and water−metal interaction energies. In previous DFT calculations, wettability of noble metal surfaces (23, 24) was defined as the ratio between the hydrogen bonding interaction energy and the adsorption energy to the surface, showing that in the case of Au(111), water−water interactions dominate. Wetted structures were observed experimentally for more reactive metals, as reviewed (25), and also most recently compared to DFT computations (26). The effects of stepped surfaces with possibly stronger binding, as proposed for methylamine adsorption (27), also have to be considered.

In this work, we examined interface interactions between side chains of selected single amino acids on gold or palladium metal cluster models to better explain peptide specificity to the surface, preliminarily for selected amino acids that constitute, in part, the sequences Flg and A3, also including water molecules. In the first stage, the objective was to examine by first principles the intrinsic relative affinity of charged side chains to the metal surface, as compared to results using an empirical potential, notwithstanding that static model compounds were modeled, charge screening, for example, was not fully into account, ideal surfaces were considered and surface diffusivity not addressed. Although conformational entropy would play a role, in this work, we aimed to estimate the relative intrinsic specificity demonstrated experimentally, such as possible "hooking" of a charged side chain to the surface, rather than general features that are dependent on the parametrization used that may not be fully representative of the interactions at the interface. This was explained, for example when using coarse-grain Monte Carlo (MC) simulations for peptides adsorbed on single-wall carbon nanotubes (28). End groups might play a role, but once again, understanding of the experimentally observed side-chain specificity was the primary goal in this case. We showed that charged residues demonstrate a stronger binding due to charge transfer, whereas polar residues reveal larger binding energies than do nonpolar residues, qualitatively reproducing the differential adhesion trend observed experimentally (9). Inclusion of dispersion effects in the DFT functional, to enable an accurate estimation of the relative contributions upon binding on periodic slabs, systematically for all naturally occurring amino acids, will be carried out in future work. Finally, the larger calculated binding energies at a Pd interface were also consistent with experimental observations.

Table 1. Adsorption of (1−6) Water Molecules on a Au(111) Surface (Pd Results in Parentheses)

Au (Pd)	d(M−O) (Å)	E_{ads} (kcal/mol)[a]	E_{ads} (kcal/mol)[b]
H_2O−1	2.84	−3.95	
H_2O−1 (PDFT)	2.78 (−2.33)	−3.77 (−8.27)	−2.42 (−7.01)
(H_2O)−2	2.61	−7.40	
(H_2O)−2 (PDFT)	2.61 (−2.34)	−7.45 (−16.60)	−5.97
(H_2O)−3	2.48	−7.55	
(H_2O)−3 (PDFT)	2.47 (−2.25)	−8.06 (−23.44)	−6.53
(H_2O)−6 (PDFT)	2.41	−9.75	−9.27

[a] $E_{ads} = E(M + nH_2O) - E(M) - E(nH_2O)$. [b] See ref 23.

COMPUTATIONAL DETAILS

Calculations were carried out using DFT because of the size of the problem in DMol3 (29), applying the PW91 exchange-correlation functional (30), for comparison with previous calculations on water adsorption (23). Numerical basis sets were used. Relativistic effective core potentials (31) were applied for Pd. Hirshfeld (32) partial atomic charges were calculated because they have been shown to be more basis-size-independent than Mulliken population analyses (33).

Side-chain adsorption on the metal surface was considered, in order to probe the experimentally observed specificity (9). The surface was modeled by a cluster consisting of 3 layers of 4 × 4 atoms cut from Au(111), and similarly for a Pd(111) surface, which we considered for additional comparison with experiment. Recent calculations confirmed that a truncated octahedron is the most stable structure for larger gold nanoparticles (≳1.5 nm), in agreement with experimental observations (34). Binding at an Au(111)/(111) ridge was modeled by 3 layers of 6 × 4 Au atoms each, with the top layer half removed. Note that the cluster was kept fixed to eliminate spurious finite cluster effects, unless noted otherwise.

Model slabs were considered by periodic (PDFT) calculations for validation, where the supercell similarly consists of 3 layers of 4 × 4 Au atoms, with a separation of about 13 Å, resulting in an Au−Au distance of 2.98 Å, consistent with experiment (35). For further validation, calculations of the adsorption of water molecules on Au(111) were also carried out (cf. Table 1), showing our results to be consistent with previous work (23), with a small disparity that could be due to the use of atomic orbitals.

RESULTS AND DISCUSSION

Optimized geometries of single amino acids, including Asp, Lys, Arg, Ser, Pro, and Val, on an ideal Au(111) surface, in order to better understand side-chain specificity of Flg, A3, including selected amino acids for comparison, were determined after some configurational space exploration,

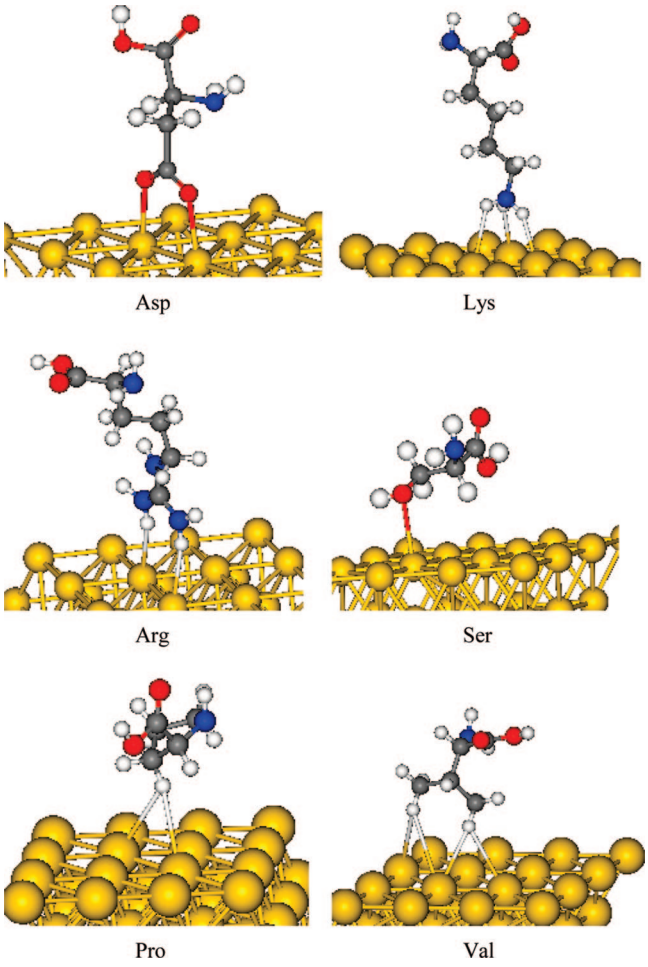

FIGURE 1. Optimized geometries of amino acids adsorbed on an Au(111) cluster surface. Lines denote distances as discussed in the text.

although no comprehensive search was carried out by ab initio MD simulations. For example, for Asp, several initial positions of O atoms on the Au(111) surface were examined, namely, placed midpoint between two Au atoms, at the center of the triangle formed by three Au atoms, and at the center of the rectangle formed by four Au atoms, where in all cases geometry optimization resulted in the oxygen atop an Au atom. For Asp, Lys, Arg, and Ser, the side-chain atoms adsorb on top of an Au atom (cf. Figure 1), whereas the closest H atoms in Pro and Val are situated at a bridge position, i.e., between two metal atoms (distances are denoted in Figure 1, and the results are summarized in Table 2). Because experimental measurements (9) were carried out at neutral pH, Asp assumes a negative charge and Lys and Arg are positive. For the neutral amino acids, geometrical parameters were consistent with previous electronic structure calculations (36). Adsorption distances are shortened upon charge transfer for charged residues, as compared to weaker physisorption. In addition, slightly shorter distances were consistently observed upon relaxation of the top layer, both for nonperiodic and periodic calculations.

The adsorption energy of a side-chain amino acid (A) on an ideal metal surface (M) was defined as $E_{ads} = E(M + A) - E(M) - E(A)$. The results are summarized in Table 2. The adsorption energies for charged residues were noted to be significantly larger, namely of −57, −27, and −19 kcal/mol for Asp, Lys, and Arg respectively, than those of −6, −4, and −3 kcal/mol, for Ser, Pro, and Val, respectively. The calculated adsorption energies using the consistent valence force field (CVFF) empirical potential energy function were −24, −16, −13, −12, and −19 kcal/mol, for the amino acids Asp, Lys, Arg, Pro, and Val, respectively, therefore not reproducing the experimentally observed trend in adhesion specificity (9). Shortcomings of existing Lennard−Jones potentials were recently pointed out, and improved upon by fitting to experimental surface tension data (37). However, charge transfer and exchange interactions upon adsorption on a metal surface are still not taken into account adequately. Calculation of the carboxylic and amine end groups' adsorption to the gold surface as compared to the Asp side chain resulted in smaller adsorption energies by about 20 kcal/mol, consistent with the experimentally observed specificity. Stronger adsorption is observed at an Au (111)/(111) ridge (see Table 2; the optimized structures are shown in Figure 2), consistent with a previous observation for molecular adsorption (27). An alternative positioning of the amino acids at the ridge was considered by changing the orientation of the side chain relative to the step, resulting in similar adsorption energies, of −70, −18, −7, −4 kcal/mol, for Asp, Arg, Ser, and Val, respectively. Once again, the DFT results are qualitatively consistent with the experimental trend (9), contrary to the empirical CVFF values. Note that results for the adsorption of uncharged amino acids on cluster models were also consistent with corresponding calculations for model periodic slabs (Table 2), further validating the use of a cluster model in those cases. The calculated partial atomic charge on the Au(111) cluster for Asp adsorption, of about −0.65e, showed considerable charge transfer, whereas neutralizing the charged residues clearly led to a decrease in the binding energy, as expected. Charge transfer of about 0.4e was calculated for Lys and Arg. Interestingly, it was experimentally observed (9) that a decrease in the adhesion of His and Lys 10-mers on a Si_3N_4 surface is noted when the pH of the solution was increased beyond the pK_a, thus neutralizing the basic amino acids. As mentioned, adsorption energies for charged side-chain residues are overestimated because charge screening due to the environment has not been taken into account. Note that increased ionic strength was not reported experimentally (9).

In the case of charged residues, charge transfer clearly dominates binding, but quantitatively determining the relative strength of interactions would require comprehensive simulations, with better treatment of the environment. The stronger binding of the charged residues in Flg, as compared to Ser and Pro in A3, could explain, in part, the larger aggregates noticed upon gold precipitation by Flg (8). Upon physisorption, the relative order of E_{ads} for Ser, Pro, and Val follows the trend in the amino acids' polarizability (38). Charge transfer was negligible for these amino acids, less than 0.1e. Adsorption of A3 on the gold nanoparticle surface is sparse (ca. 12 peptides on a 12 nm particle) (10), and therefore surface dipole−dipole interactions would not play a role.

Table 2. E_{ads}(kcal/mol), Distance (Å) between the Au(111) Cluster Surface and the Heavy Atom in an Amino Acid (A) and Hydrogen Atom (H)

	charge	d(M−A)	d(M−H)	E_{ads}
Asp	−1 (0)[a]	2.31 (4.74)[a] (2.23)[c]		−56.7 (−0.6)[a] (−28)[b] (−70.2,−49[b])[c]
Lys	+1 (0)[a]	3.34 (2.66)[a] (3.43)[c]	2.50	−26.7 (−4.9)[a] (−16)[b] (−26.7)[c]
Arg	+1	3.53	2.58	−18.8 (−13)[b]
Ser	0	3.04[a]	3.02[a]	−5.7
Pro	0	3.97 (3.97)[a] (3.88, 3.84[b])[c]	3.24 (3.24)[a]	−4.3 (−4.1)[a] (−12)[b] (−3.4,−4.0[a],−37[b])[c]
Val	0	3.96 (3.95)[a] (3.91, 3.99[b])[c]	3.06 (3.06)[a]	−2.9 (−2.7)[a] (−19)[b] (−2.9)[c]

[a] PDFT. [b] CVFF. [c] Binding at an Au ridge (111)/(111).

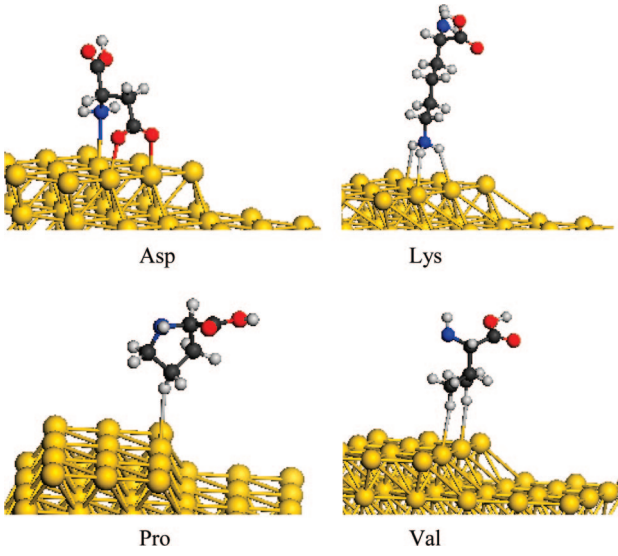

FIGURE 2. Optimized geometries of amino acids at an Au(111)/(111) ridge. Lines denote distances as discussed in the text.

To assess to some extent solvation, we carried out geometry optimizations of amino acids adsorbed on a Au(111) cluster surface including water molecules, oriented to facilitate hydrogen bonding (denoted by lines in Figure 3). Adsorption energies are summarized in Table 3. The propensity of the amino acid's side chain to adhere to the surface depends not only on the binding at the metal but also on its solvation in water, as defined by $E^{sol} = E(A + nH_2O) - E(nH_2O) - E(A)$. In normalizing to the same number of water molecules for the amino acids, the trend is consistent with expected hydration energies (39), e.g., for Lys and Asp vs Ser, and larger than the adsorption of H_2O on the metal surface (23). In an effort to assess qualitatively competing driving forces, we defined adsorption energies as $E_{ads}^{sol1} = E[M + A + nH_2O] - E[M + nH_2O] - E[A]$ and $E_{ads}^{sol2} = E[M + A + nH_2O] - E[A + nH_2O] - E[M]$. A larger value of E_{ads}^{sol1} as compared to E_{ads}^{sol2} would indicate that the binding is driven by anchoring to the surface, while a larger value of E_{ads}^{sol2} emphasizes the importance of hydration. For example, in comparing adhesion of Asp and Arg, as shown in Table 3, E_{ads}^{sol2} is smaller or comparable to E_{ads}^{sol1}, respectively, demonstrating a specificity of binding through side-chain adhesion for Asp, whereas weak adhesion, possibly mediated by water, is indicated for the positively charged residue.

The difference between Arg and Lys binding (9) is still unclear and will require further experimental investigation. Overall, however, the binding on a gold surface is weak, as

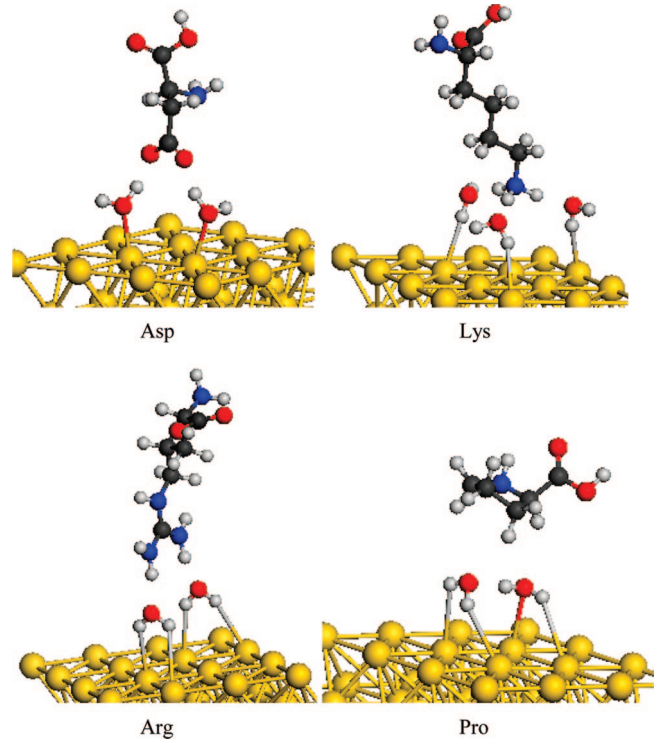

FIGURE 3. Optimized geometries of amino acid absorbed on a wetted Au(111) cluster surface. Lines denote distances as discussed in the text.

Table 3. Adsorption Energies (kcal/mol) (Definition Given in Text), Distances (Å) between Au(111) Cluster Surface and O, H of Water, and Heavy Atom in A[a]

	d(M−O)	d(M−H)	d(M−A)	E_{ads}^{sol1}	E_{ads}^{sol2}	E^{sol}
Asp	2.42−2.47	2.76−3.22	4.55	−49.7	−31.0	−34.4
Lys	3.38−3.55	2.41−3.62	4.25	−38.2	−21.7	−46.0
Arg	3.49−3.50	2.66−3.13	5.06	−25.1	−14.3	−26.7
Pro	2.78−3.43	2.93−3.08	5.43	−3.1	−11.2	−7.8
Ser	2.78−3.48	3.02−3.31	4.66	−12.7	−14.9	−9.1

[a] The range of distances denotes varying potential adsorption sites of water molecules, with the reported adsorption energies given for the lowest energy configuration.

observed in comparing experimentally the results for different solvents, namely, H_2O, HEPES buffer, and DMSO (9). In HEPES, the adhesion characteristics of Lys and Arg are reversed as compared to an aqueous solution whereas not notable for either in DMSO. Adhesion in DMSO, retained only for Asp (9), is consistent with the larger adsorption energy predicted computationally. Note that the pK_a of Arg

is larger than that of Lys. Interestingly, for Tyr, where the hydration energy is relatively large (35), adhesion on a gold surface is expected to be reduced, as was indeed observed experimentally (9). Of course, effects of solvent are complicated, as demonstrated even for these solvents, and would require further computational and experimental investigation. However, the intrinsic binding is delineated, and the trend is in qualitative agreement with experiment.

Adsorption characteristics for a Pd(111) cluster surface, corresponding to the Au(111) optimized configurations, show stronger adsorption, accompanied by shortened distances. For instance, the calculated values of E_{ads} for Asp and Lys, of −69, and −34 kcal/mol, respectively, in the gas phase, as compared to the corresponding values for a gold surface, of −57, −27 kcal/mol, respectively, are qualitatively consistent with experiment (9). Similarly, for example, results of E_{ads}^{sol} of −52, −50 kcal/mol for Asp and Lys, respectively, as compared to adsorption at the Au(111) surface, of −50, −38 kcal/mol, respectively, are shown to be larger. Indeed, overall binding energies at the Pd interface are larger than for Au because of the more reactive Pd surface, consistent with the results for water adsorption (cf. Table 1), as expected, and recently pointed out (26). Interestingly, when experimentally exposing a Pd surface to gold nanoparticles coated with either A3, Flg-A3, or A3-Flg, those coated with Flg-A3 were found to have the largest remaining number on the Pd nanoparticle surface after several wash cycles (11). Once again, because the Flg (-Asp-Tyr-Lys-Asp-Asp-Asp-Asp-Lys-) sequence consists of Asp and Lys amino acids while A3 (-Ala-Tyr-Ser-Ser-Gly-Ala-Pro-Pro-Met-Pro-Pro-Phe-) contains only uncharged residues, the larger observed affinity of Flg to the Pd surface was consistent with our results.

CONCLUSION

In examining the adsorption of amino acids on Au and Pd model surfaces by applying DFT calculations, we have shown that charged residues demonstrate a stronger specific binding because of charge transfer, whereas tuning the pH of the solution could change the binding affinity. Polar residues demonstrate larger binding energies than nonpolar residues. A larger binding energy at the Pd surface than at an Au surface for charged residues was also calculated. Moreover, for the weakly binding side chains, the interplay between amino acid solvation and adsorption at the surface was considered, showing that a change in the solvent could be an additional parameter in designing peptides for metal surface adhesion.

This work serves as the first step toward gaining an understanding of specific interactions of biological nanostructures at a metal interface, for example in attempting to explain adhesion of Flg and A3 to Au and Pd nanoparticle surfaces, in which the importance of applying first-principles calculations and taking into account the effects of the environment were emphasized. Simulations of peptide adsorption will be carried out in future work, to further understand the effects of amino acid composition on metal surface adsorption, using functionals that take into account dispersion (18).

Acknowledgment. G. Hong acknowledges partial support of a NRC RAP fellowship. The DoD High Performance Computing Modernization Program is gratefully acknowledged for computer time and the AFRL Major Shared Resource Center for helpful support. B. Akdim is acknowledged for helpful discussions. Insightful comments by the referees are thankfully acknowledged.

REFERENCES AND NOTES

(1) Feldheim, D. L.; Eaton, B. E. *ACS Nano* **2007**, *1*, 154–159.
(2) Baron, R.; Willner, B.; Willner, I. *Chem. Comm.* **2007**, 323–332.
(3) Slocik, J. M.; Naik, R. R. *Curr. Nanosci.* **2007**, *3*, 117–120.
(4) Merzlyak, A.; Lee, S.-W. *Curr. Opin. Chem. Biol.* **2006**, *10*, 246–252.
(5) Willner, I.; Baron, R.; Willner, B. *Biosens. Bioelectron.* **2007**, *22*, 1841–1852.
(6) Astier, Y.; Bayley, H.; Howorka, S. *Curr. Opin. Chem. Biol.* **2005**, *9*, 576–584.
(7) Peelle, B. R.; Krauland, E. M.; Wittrup, K. D.; Belcher, A. M. *Langmuir* **2005**, *21*, 6929–6933.
(8) Slocik, J. M.; Stone, M. O.; Naik, R. R. *Small* **2005**, *1*, 1048–1052.
(9) Willett, R. L.; Baldwin, K. W.; West, K. W.; Pfeiffer, L. N. *Proc. Nat. Acad. Sci. U.S.A.* **2005**, *102*, 7817–7822.
(10) Slocik, J. M.; Naik, R. R. Personal communication.
(11) Slocik, J. M.; Naik, R. R. *Adv. Mater.* **2006**, *18*, 1988–1992.
(12) Braun, R.; Sarikaya, M.; Schulten, K. *Biomater. Sci. Polym. Ed.* **2002**, *13*, 747.
(13) Harding, J. H.; Duffy, D. M. *J. Mater. Chem.* **2006**, *16*, 1105–1112.
(14) Schravendijk, P.; Ghiringhelli, L. M.; Delle Site, L.; van der Vegt, N. F. A. *J. Phys. Chem. C* **2007**, *111*, 2631–2642.
(15) Bocquet, M.-L.; Rappe, A. M.; Dai, H.-L. *Mol. Phys.* **2005**, *103*, 883–890.
(16) Bagus, P. S.; Staemmler, V.; Woll, C. *Phys. Rev. Lett.* **2002**, *89*, 0961041−0961044.
(17) Rusu, P. C.; Giovannetti, G.; Brocks, G. J. *Phys. Chem. C* **2007**, *111*, 14448–14456.
(18) Wu, Q.; Yang, W. *J. Chem. Phys.* **2002**, *116*, 515–524.
(19) Choe, W.-S.; Sastry, M. S. R.; Thai, C. K.; Dai, H.; Schwartz, D. T.; Baneyx, F. *Langmuir* **2007**, *23*, 11347–11350.
(20) Patwardhan, Si V.; Patwardhan, G.; Perry, C. C. *J. Mater. Chem.* **2007**, *17*, 2875–2884.
(21) Kilina, S.; Tretiak, S.; Yarotski, D. A.; Zhu, J.-X.; Modine, N.; Taylor, A.; Balatsky, A. V. *J. Phys. Chem. C* **2007**, *111*, 14541–14551.
(22) Meng, S. Wang, W. L. Maragakis, P. Kaxiras, E. *Nano Lett.* (**2007**), *7*, 2312−2316.
(23) Meng, S.; Wang, E. G.; Gao, S. *J. Chem. Phys.* **2003**, *119*, 7617–7620.
(24) Meng, S.; Wang, E. G.; Gao, S. *Phys. Rev. B* **2004**, *69*, 195404/1–195404/13.
(25) Michaelides, A. *Appl. Phys. A* **2006**, *85*, 415–425.
(26) Michaelides, A.; Morgenstern, K. *Nat. Mater. (* **2007**, *6*, 597–601.
(27) Pong, B.-K.; Lee, J.-Y.; Trout, B. L. *Langmuir* **2005**, *21*, 11599–1603.
(28) Cheng, Y.; Liu, G. R.; Li, Z. R.; Lu, C.; Mi, D. *J. Phys. D: Appl. Phys.* **2008**, *41*, 055308.
(29) (a) Delley, B. *J. Chem. Phys.* **1990**, *92*, 508–517. (b) Delley, B. *J. Chem. Phys.* **2000**, *113*, 37756–7764, as implemented in DMol3 by Accelrys, Inc. .
(30) Wang, Y.; Perdew, J. P. *Phys. Rev. B* **1992**, *45*, 13244–13249.
(31) (a) Dolg, M.; Wedig, U.; Stoll, H.; Preuss, H. J. *Chem. Phys.* **1987**, *86*, 866–872. (b) Bergner, A.; Dolg, M.; Kuechle, W.; Stoll, H.; Preuss, H. *Mol. Phys.* **1993**, *80*, 1431–1441. (c) Andrae, D.; Häussermann, U.; Dolg, M.; Stoll, H.; Preuss, H. *Theor. Chim. Acta* **1990**, *77*, 123–141.
(32) Hirshfeld, F. L. *Theor. Chim. Acta* **1977**, *44*, 129–138.
(33) Guerra, C. F.; Handgraaf, J.-W.; Baerends, E. J.; Bickelhaupt, F. M. *J. Comp. Chem.* **2003**, *25*, 189–210.
(34) Barnard, A. S.; Curtiss, L. A. *ChemPhysChem* **2006**, *7*, 1544–1553.
(35) Kittel, C. *Introduction to Solid State Physics*; Wiley: New York, 1986.
(36) Millefiori, S.; Alparone, A.; Millefiori, A.; Vanella, A. *Biophys. Chem.* **2008**, *132*, 139–147.
(37) Heinz, H.; Vaia, R. A.; Farmer, B. L.; Naik, R. R. *J. Phys. Chem. C* **2008**, *112*, 17281–17290.
(38) Song, X. *J. Chem. Phys.* **2002**, *116*, 9359–9363.
(39) Wolfenden, R.; Andersson, L.; Cullis, P. M.; Southgate, C. C. B. *Biochemistry* **1981**, *20*, 849–855.

AM800099Z